Performance Characterization of a Multiplexed Space-to-Ground Optical Network

Marc Sanchez Net, Iñigo del Portillo, Bruce Cameron, Edward Crawley
Massachusetts Institute of Technology
77 Massachusetts Ave 33-409
Cambridge, MA 02139
617-682-6521
{msnet,portillo,bcameron,crawley}@mit.edu

***Abstract*—Advances in phased array systems for multi-beam free space optical communications are a key enabler for a new space-to-ground network architecture, namely a multiplexed optical architecture. The fundamental idea of a multiplexed space-to-ground optical network is the utilization of a multi-beam optical payload that allows each spacecraft to establish links with multiple ground stations within its line of sight. Information is then downlinked in parallel, from the satellite to the ground, through the subset of links not disrupted by clouds.**

In this paper we evaluate the performance of a multiplexed optical space-to-ground architecture from a systems perspective, with particular emphasis on the effect of cloud correlation in the network throughput. In particular, we first derive the expected data volume returned in a multiplexed architecture as a function of the optical network availability and the system total capacity. Then, we compare the performance of the proposed multiplexed architecture against a traditional single-beam downlink system that utilizes site diversity to mitigate cloud coverage effects. This comparison is based on two canonical scenarios, a global highly uncorrelated network representative of a geosynchronous satellite; and local, highly correlated, network representative of a low Earth orbit spacecraft. Through this analysis, we demonstrate that multiplexed architectures can improve the throughput of a space-to-ground optical network as compared to that of a single ground telescope without requiring a beam switching mechanism.

TABLE OF CONTENTS

1. INTRODUCTION

Optical communications are an upcoming technology that can revolutionize the amount of information that can be sent to and from space in the upcoming decades (see, for instance, [1]). That being said, they also suffer from limitations that are not problematic for traditional radio-frequency communications. Among them is the sensitivity of optical space-to-ground links to disruptions from atmospheric impairments, most notably clouds.

978-1-5090-1613-6/17/31.00

Literature Review

Many references have studied the effect of clouds on space-to-ground optical networks. For instance, References [2] and [3] utilize the Lasercom Network Optimization Tool (LNOT) to determine the optimal locations for ground telescopes that provide service to a deep space probe. The key metric they optimize is *optical network availability*, i.e. the probability of having at least one link not disrupted by clouds. Similar studies are have also been performed by European institutions [4], [5], as well as their Japanese counterparts [6].

Other references have centered their attention towards characterizing the amount of data that can be returned from space using optical communication systems. In that sense, the Optical Link Study Group provided a seminal reference in which they analyzed the performance of optical networks with respect to the percent data transfered [7]. In their view, the fundamental metric to be optimized when designing a space-to-ground optical communication network is data volume, specifically the probability of successfully transmitting certain percent of data collected by the spacecraft. Nonetheless, their work is restricted to understanding the performance of a single access payload, i.e. a laser that can communicate with one ground station at a time.

Optical beam-forming systems for fast multiple access systems have already been proposed in the literature [8]. Evolution of this technology is a key enabler for a new type of space-to-ground optical system, namely a multiplexed network [9]. While the concept of a multiplexed space-to-ground optical network is not new, characterization of its data volume and comparison with the traditional single access optical system has not been performed. This paper provides a first high level comparison between these two types of optical communication systems.

Research Goals

Three main research objectives are addressed by this paper: First, derive the expected data volume per pass returned using a space-to-ground optical network assuming both an idealized single and multiple access space terminal. Second, quantify the difference in performance between both types of networks when supporting a geosynchronous and low Earth orbit customer. Finally, estimate the performance degradation of the latter customer type due to higher atmospheric correlation across telescopes in the ground segment.

Paper Structure

The remainder of this paper is structured as follows: Section 2 tackles the first research objective by proposing a simplified model for space-to-ground optical networks and providing expressions for the data volume that a spacecraft can return.

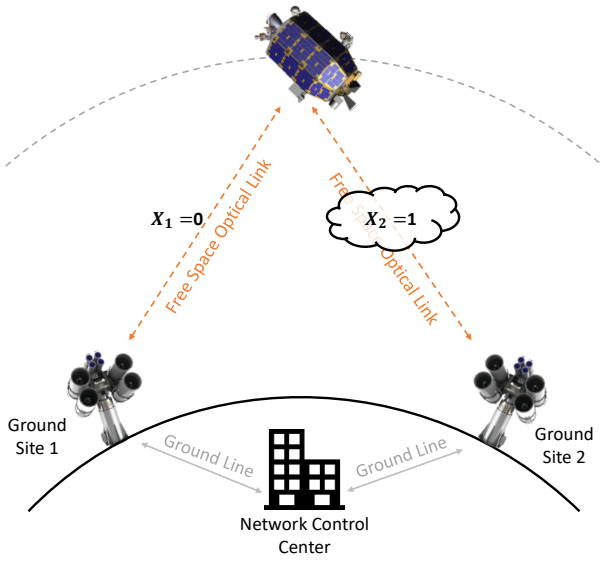

Figure 1: **Model of an Optical Network**

It also includes a brief discussion on how to use the cloud fraction data set a source of atmospheric information. On the other hand, Section 3 describes a simple model to assess the cost an optical ground network based on the number of ground stations and their location. Finally, Sections 4 and 5 evaluate the performance of a link-switched and multiplexed network architecture when supporting a geosynchronous and low Earth orbit satellite respectively. Finally, the paper concludes with a summary of results and delineation of possible lines of future work.

2. Network and Cloud Modeling

Optical Network Model

We consider the simplest possible model for a space-to-ground optical communication network: At time t, N ground stations are within line-of-sight from a spacecraft. They all have an optical telescope that can be used to establish an optical link with the spacecraft, and are interconnected with one another through ground lines (see Figure 1). Each free space optical link is modeled using a binary ON/OFF channel characterized by the probability of having a cloud disrupting it [10]. Mathematically, let $\mathcal{X}_{i,t}$ denote the random variable that models the state of the optical space-to-ground link at time t for the i-th ground station. Then, $\mathcal{X}_{i,t}$ is Bernoulli distributed as long as the ground station is in line-of-sight:

$$\mathcal{X}_{i,t} = \begin{cases} 1 & \text{with prob. } p_{i,t} \\ 0 & \text{with prob. } 1 - p_{i,t} \end{cases} \forall i \in [1, N]\,. \tag{1}$$

Let $\mathcal{X}_t$ denote the state of the entire network, i.e. the random variable that models the number of optical links that are disrupted by a cloud at time t. It is immediate to see that $\mathcal{X}_t$ can simply be estimated as the sum of $\mathcal{X}_{i,t}$ over all ground stations in visibility:

$$\mathcal{X}_t = \sum_{i=1}^{N} \mathcal{X}_{i,t}. \tag{2}$$

Furthermore, since the link outage probability (LOP) is defined as the probability of having all links clouded, it can be simply computed as

$$\text{LOP}_t = f_{\mathcal{X}}\left(X_t = N\right) = \mathcal{P}\left(\mathcal{X}_t = N\right). \tag{3}$$

Similarly, the Optical Network Availability (ONA) is defined as the probability of having at least one link available and, therefore, can be estimated as the complement of the LOP:

$$\text{ONA}_t = 1 - \text{LOP}_t. \tag{4}$$

Link-Switched Optical Network Architecture

The traditional architecture to mitigate the effect of clouds in space-to-ground optical communications assumes a linked-switched strategy. In other words, as the spacecraft moves across its orbit it selects one of the ground stations in visibility and maintains the laser locked onto it until it either becomes clouded or it is occulted by the Earth horizon. At that point, the beam is switched to another non-clouded ground station, a process that we assume instantaneous and error-free to simplify the analysis.

Let $\mathcal{D}_s$ denote the random variable that models the data volume returned over a pass measured in bits. Assume that this pass has a total duration of T seconds and an average data rate of R_b bits per second. Then, between instants t and $t + dt$ the total data volume returned through the optical link is $R_b \cdot dt$ if $\mathcal{X}_t < N$ and zero otherwise. Consequently

$$\mathcal{D}_s = \int_{t_0}^{t_0+T} R_b \mathbb{1}_{\mathcal{X}_t < N} d\tau, \tag{5}$$

where $\mathbb{1}_{\mathcal{X}_t<N}$ denotes the indicator function over the set $\{\mathcal{X}_t < N\} = \{0, 1, 2, ..., N-1\}$, and t_0 denotes the arbitrary time instant in which the pass starts. Assuming that during the T seconds of a pass the N ground stations in line-of-sight are constant, we can compute the expected data volume returned over the pass as

$$\begin{aligned} \mathrm{E}\left[\mathcal{D}_s\right] =& \mathrm{E}\left[\int_{t_0}^{t_0+T} R_b \mathbb{1}_{\mathcal{X}_t<N} d\tau\right] = R_b \int_{t_0}^{t_0+T} \mathrm{E}\left[\mathbb{1}_{\mathcal{X}_t<N}\right] d\tau = \\ =& R_b \int_{t_0}^{t_0+T} \sum_{i=0}^{N-1} \mathcal{P}\left(\mathcal{X}_t = i\right) d\tau = \\ =& R_b \int_{t_0}^{t_0+T} \left[1 - \mathcal{P}\left(\mathcal{X}_t = N\right)\right] d\tau = R_b \int_{t_0}^{t_0+T} \text{ONA}_t d\tau. \end{aligned} \tag{6}$$

Finally, assuming that ONA_t is stationary during T seconds (which is always the case unless the contact duration was set to days at a time), we estimate the expected data volume returned per pass in a link-switched optical network architecture as:

$$D_s(t) = \mathrm{E}\left[\mathcal{D}_s\right] = R_b \cdot T \cdot ONA_t. \tag{7}$$

Multiplexed Optical Network Architecture

In a multiplexed optical network the spacecraft has the ability to establish multiple space-to-ground links simultaneously

with spatially-diverse ground stations. Assume no restrictions on the number of simultaneous links that can be established. Then, at each instant of time, a pass returns a total data volume of $R_b \cdot [N - X_t] \cdot dt$ bits, where $[N - X_t]$ denotes the number of links that are not clouded at time t over the N sites that are in line-of-sight from the spacecraft. Consequently, the total data volume per pass can be expressed as

$$\mathcal{D}_m = \int_{t_0}^{t_0+T} R_b \left[N - \mathcal{X}_t\right] d\tau. \tag{8}$$

Once again assuming stationarity of $\mathcal{X}_t$ over T seconds and constant N, the expected data volume over a pass can be simply estimated as

$$\begin{aligned} D_m(t) =& \mathrm{E}\left[\mathcal{D}_m\right] = \mathrm{E}\left[\int_{t_0}^{t_0+T} R_b \left[N - \mathcal{X}_t\right] d\tau\right] = \\ =& \int_{t_0}^{t_0+T} R_b \left[N - \mathrm{E}\left[\mathcal{X}_t\right]\right] d\tau = \\ =& R_b \cdot \left[N - \bar{X}_t\right] \cdot T, \end{aligned} \tag{9}$$

where $\bar{X}_t$ denotes the average number of links clouded at time t given the ground stations in visibility and their local yearly seasonality.

Normalized Network Throughput and Multiplexing Efficiency

Equations 7 and 9 provide the analytic expression for the expected data volume per pass for a link-switched and multiplexed optical space network. They depend on the supportable link data rate and contact time, both of which are not directly affected by the cloud probabilities. Furthermore, in the multiplexed architecture we have assumed that N optical links can be established at the same time. Therefore, the data rate per link should be reduced by a factor N as compared to the linked-switched architecture or else the total system capacity will be N times larger (and so will be the power requirements of the spacecraft). Taking these considerations into account, we define the normalized network throughput as

$$D_s = \frac{1}{T_m} \int_{t_0}^{t_0+T_m} \frac{D_s(t)}{R_b \cdot T} \approx \frac{1}{T_m} \sum_{t=t_0}^{t_0+T_m} \mathrm{ONA}_t, \tag{10}$$

$$D_m = \frac{1}{T_m} \int_{t_0}^{t_0+T_m} \frac{D_m(t)}{R_b \cdot T} \approx \frac{1}{T_m} \sum_{t=t_0}^{t_0+T_m} \frac{N - \bar{X}_t}{N}, \tag{11}$$

where T_m is used to indicate the total mission operation time and the N factor in Equation 11's denominator is included to indicate that the data rate per beam is N times lower. Note that both D_s and D_m do not take into account any operational factors and only depend on the network architecture, i.e. how many ground stations are available, whether they are correlated or not, and how clouded they are.

Finally, since we would like to compare the performance of a multiplexed and link-switched architecture, we also define the normalized multiplexing efficiency as

$$\eta = \frac{D_m}{D_s} = \frac{\sum_{t=t_0}^{t_0+T_m} 1 - \frac{\bar{X}_t}{N}}{\sum_{t=t_0}^{t_0+T_m} \mathrm{ONA}_t}. \tag{12}$$

It quantifies the expected relative increase/decrease in data volume returned if a mission is supported using a multiplexed optical network architecture, instead of a traditional link-switched architecture. Evidently, in a world without clouds $\eta = 1$, i.e. since the $\mathrm{ONA} = 1$ and $\bar{X}_t = 0$.

Estimating the Cloud Fraction Probability

Once the expressions for the normalized network throughput and multiplexing efficiency have been derived, we now provide a succinct explanation on how to estimate the state of an optical network $\mathcal{X}_t$ and its characteristic properties ONA_t and $\bar{X}_t$. This summary is primarily based on the cloud modeling discussion from Sanchez Net *et al.* in Reference [10]. An exhaustive description and derivation of the equations herein summarized is provided in that reference.

The first step to determine the state of any given optical network is to estimate the cloud probabilities of each ground site p_i. To that end, we utilize the preprocessed cloud fraction data product (see Figure 2 adapted from Reference [10]) from NASA's Terra and Aqua satellites [13]. It is provided as a set of geolocated and time stamped images available on a daily basis starting from the year 2000. Each pixel in the image has a value between 0 and 1 assigned to it that indicates the probability of having a cloud in that position. Additionally, weekly and monthly averages are also available.

Let $\mathcal{F}(\phi, \lambda, t)$ denotes the cloud fraction at time t at a given latitude ϕ and longitude λ. Then, we estimate the steady state cloud probability for a ground station located at these coordinates as

$$p_{i,t} = \mathrm{E}_t\left[\mathcal{F}(\phi, \lambda, t)\right]. \tag{13}$$

When computing this expectation four factors have to be taken into account:

1. The pointing profile between the ground telescope and the spacecraft.
2. The possible parallax error in the cloud fraction data set.
3. The seasonality of the cloud fraction time series.
4. The spatial and temporal correlations of the cloud fraction time series.

The pointing profile between the ground telescope and the spacecraft defines which pixels in the vicinity of the ground station should be utilized to quantify the cloud fraction probability. In other words, for a site located at coordinates (ϕ, λ) we should average $\mathcal{F}(\phi, \lambda, t)$ along with the cloud fraction time series of its neighboring pixels $\mathcal{F}(\phi \pm k_1 \cdot d\phi, \lambda \pm k_2 \cdot d\lambda, t)$. Using Reference [10], we estimate the extent of this vicinity (i.e., k_1 and k_2) as all pixels within a maximum distance $d_{max} = \theta \cdot R$ from the original pixel at coordinates (ϕ, λ), with

$$\theta = \frac{\pi}{2} - \epsilon_{min} - \arcsin\left(\frac{R}{R+h}\cos\epsilon_{min}\right), \tag{14}$$

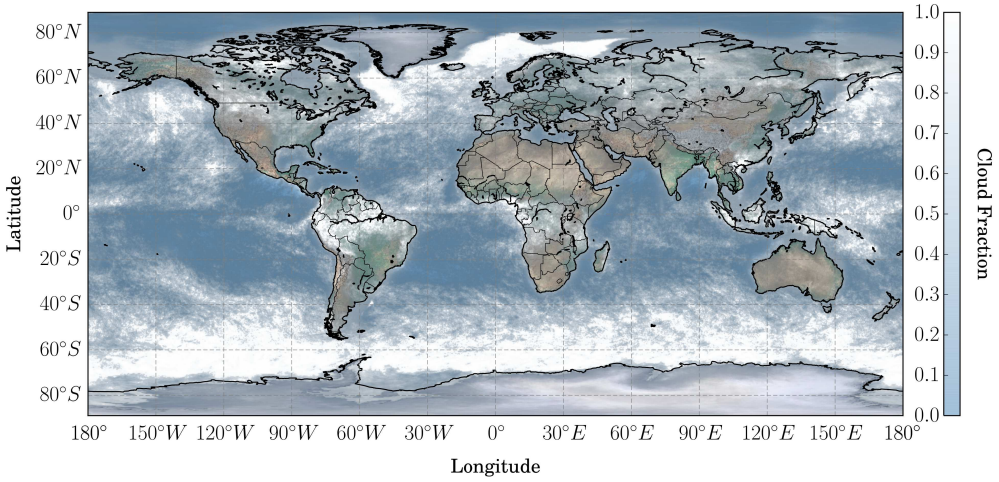

Figure 2: **Cloud Fraction Map Example**

R equal to the mean Earth radius and ϵ_{min} equal to the telescope minimum elevation angle (typically $10 - 20\,\mathrm{deg}$). For instance, a geosynchronous satellite that communicates with a telescope located at White Sands, NM and with a minimum elevation angle of $20\,\mathrm{deg}$, will require averaging a total of 13 pixels [10].

On the other hand, the parallax error refers to the position error incurred when a space-based instrument takes measurements in a direction other than spacecraft's nadir. Its maximum value is estimated to be 7.4km, less than the cloud fraction data set pixel size [10]. Therefore, it is considered a second-order effect that is already included in the averaging process due to the telescope-spacecraft pointing profile.

The cloud fraction time series is highly dependent on the site location and season (winter, spring, summer, fall). For instance, it is well-known that networks with ground sites in both the Northern and Southern Hemispheres have better availability than those with only sites in the continental United States [3]. Based on the findings of Reference [10], we will capture the effect of cloud seasonality by utilizing monthly cloud fractions and computing the network state $\mathcal{X}_t$ and returned data volume per pass on a month-by-month basis.

Finally, the spatial and temporal correlation of the cloud fraction at different locations is used to capture the notion that sites located close enough should be subject to similar cloud conditions. In that sense, spatial correlation can not be directly quantified with the cloud fraction data set as it does not indicate if two sites are clouded at exactly the same time. For that reason, a simplified exponential model is used for estimating spatial correlation between two sites:

$$\lambda_{ij} = \exp \frac{-d_{ij}}{d_0}, i, j \in [1, N], i \neq j, \tag{15}$$

with all distances expressed in kilometers. Equation 15 was first derived by Garcia [14] and empirical data indicated that the normalization factor d_0 is typically between 200 and 400km. For the purposes of this paper, an average distance of d_0 =300km was selected.

Estimating the State of an Optical Network

The cloud fraction probability $p_{i,t}$ for a given ground station, as well as its correlation with another ground station λ_{ij} are inputs to three approximation methods that can be used to estimate the probability of having a certain number of space-to-ground links clouded: $f_{\mathcal{X}}\left(X_t = N\right)$. These approximation methods include:

1. Lyapunov Central Limit Theorem (CLT).
2. Uncorrelated Monte Carlo sampling (MCS).
3. Correlated Monte Carlo sampling.

The Lyapunov CLT can be used if the spatial correlation between any two ground stations is less than 10% and N is greater than 3 sites. In other words, the network has a large number of ground stations and they are all uncorrelated to one another. In contrast, for a small network with less than 4 sites and no correlation, uncorrelated MCS should be utilized. Finally, if any two ground sites are spatially correlated, only the correlated MCS can be utilized as the other two approximations might severely overestimate the optical network availability.

To exemplify this issue, Figure 3 adapted from Reference [10] compares the result of estimating the ONA_t during 4 years using the monthly cloud fraction data set for eight different network architectures and a geostationary satellite. Four of them are uncorrelated and the other four highly correlated. In the figure, the MCS correlated and Lyapunov CLT are benchmarked against the ONA_t estimated using discrete time simulation with cloud imagery every 2 hours. Observe that in the uncorrelated cases, there is no significance difference between the approximation approaches and the discrete time simulation. In contrast, in the correlated case the Lyapunov CLT largely overestimates the ONA_t, while the correlated MCS provides results similar to the simulation benchmark.

3. NETWORK COST

In Section 2 we introduced a model to analytically estimate the normalized throughput for both a link-switched and multiplexed optical space network architecture. To understand the trade-off between this metric of performance and network cost, in this section we present a simplified model to estimate

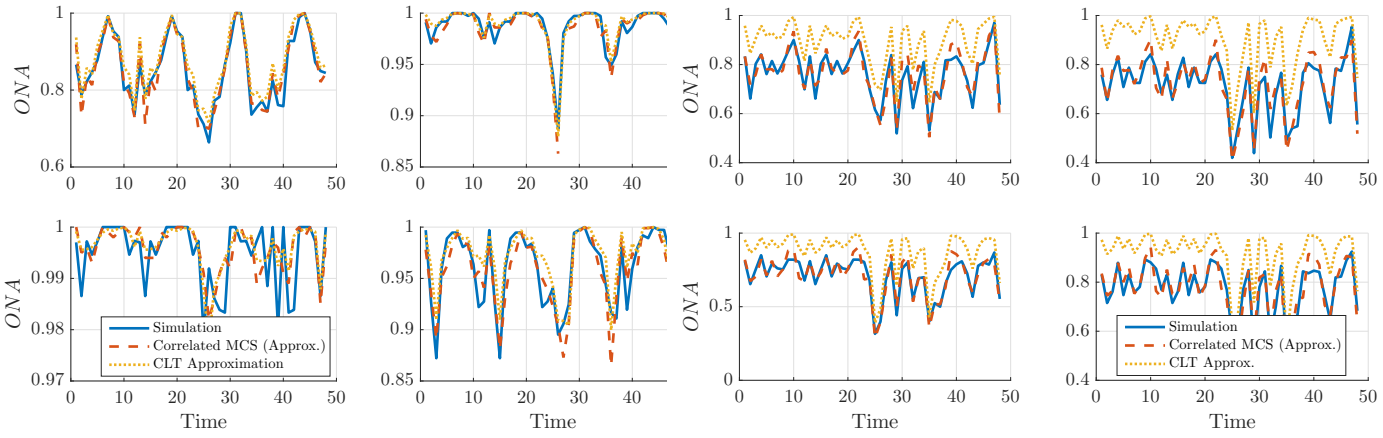

(a) **Uncorrelated Ground Telescopes** (b) **Correlated Ground Telescopes**

Figure 3: **Simulated vs. Approximated Cloud Fraction Time Series**

a ground station life cycle cost. Both normalized network throughput and life cycle cost will be utilized in Sections 4 and 5 as competing objectives to optimize the system.

Let LCC denote the ground network's cost over a $T_n = 30$ year life cycle. Then, following the insights from reference [15], we estimate the total life cycle cost for any given ground station as

$$LCC = CC + PV\{SC_t\} = CC + \sum_{t=1}^{T_n} \frac{SC_t}{(1+r)^t}, \quad (16)$$

where CC denotes the system construction cost, SC_t represents the sustainment cost (operations plus maintenance) at time t and r is the assumed discount factor to transform all cash flows to present value.

Since we are only interested in relative cost comparisons, we assume that the baseline cost of building a ground station is unitary (normalized to \$1). Three factors affect this normalized value: Location where it is built, programmatic overhead and contingency (see reference [15]). Of them, the most important are the area factors that capture the relative cost increase (or decrease) when placing a ground station at a given location in the world. As an example, ground stations in the island of Hawaii are typically twice as expensive as those in built in continental US.

On the other hand, yearly sustainment costs at any point of the system life cycle are estimated as a percentage α of the initial construction cost, corrected by both a location and an inflation factor. These last two factors are also tabulated in Reference [15], while an average yearly sustainment to construction cost fraction of 40% is estimated from the seven priced optical telescopes in reference [16]. Note that this 40% takes into account both the site operations costs, as well as leasing the communication lines that connect it with other sites and the network control center.

Table 2 in the Appendix provides the normalized life cycle cost for all ground stations considered in the geosynchronous (GEO) and low Earth orbit (LEO) scenarios.

4. GEOSYNCHRONOUS SATELLITE SCENARIO

Scenario Description

In this scenario we simulate the support of a geostationary satellite located at 90W longitude using both a link-switched and multiplexed optical space architecture. Figure 4 provides a visual representation of the candidate ground stations that can be selected in order to build a space-to-ground network, as well as the spatial correlation between them. Observe that a mix of correlated and uncorrelated ground stations are included. They are extracted from Reference [17] and contain a list of NASA ground stations and observatories that are in continuous line of sight with the geosynchronous satellite assuming a minimum elevation angle of $10\,\mathrm{deg}$.

The cloud fraction data set is processed following the steps described in Section 2, resulting in a cloud fraction time series for each ground station. As an example, Figure 5 plots the time series $p_{i,t}$ for Arequipa and Wallops during three years approximately. Note the significant differences between the cloud profile at both locations: Wallops has a cloud probability of more than 50% most of the year. In contrast, Arequipa is significantly impacted by seasonality effects, which results in May, June and July being less clouded and therefore optimal for optical communication purposes.

The architecture of the ground segment is encoded using a binary array with 17 positions, one for each ground station present in Table 2. If the i-the position is equal to 1, then that site will be built (and vice versa). Consequently, a total of $2^{17} = 131072$ alternatives can be generated. Additionally, two architectures for the space segment are possible, linked-switched or multiplexed. Thus, a total of 262144 system configurations have to be evaluated. For each of them, we utilize the pre-computed cloud fraction time series $p_{i,t}$ for the ground stations present in that architecture and estimate ONA_t and $\bar{X}_t$ using the approximation methods from Reference [10]. Finally, we compute the D_s, D_m and η using their corresponding equations, as well as the network life cycle cost.

Link-Switched vs. Multiplexed Architecture

Figure 6a plots the Pareto front (i.e. the optimal architectures) in the performance-cost space for both the multiplexed and link-switched optical communication technology. Interest-

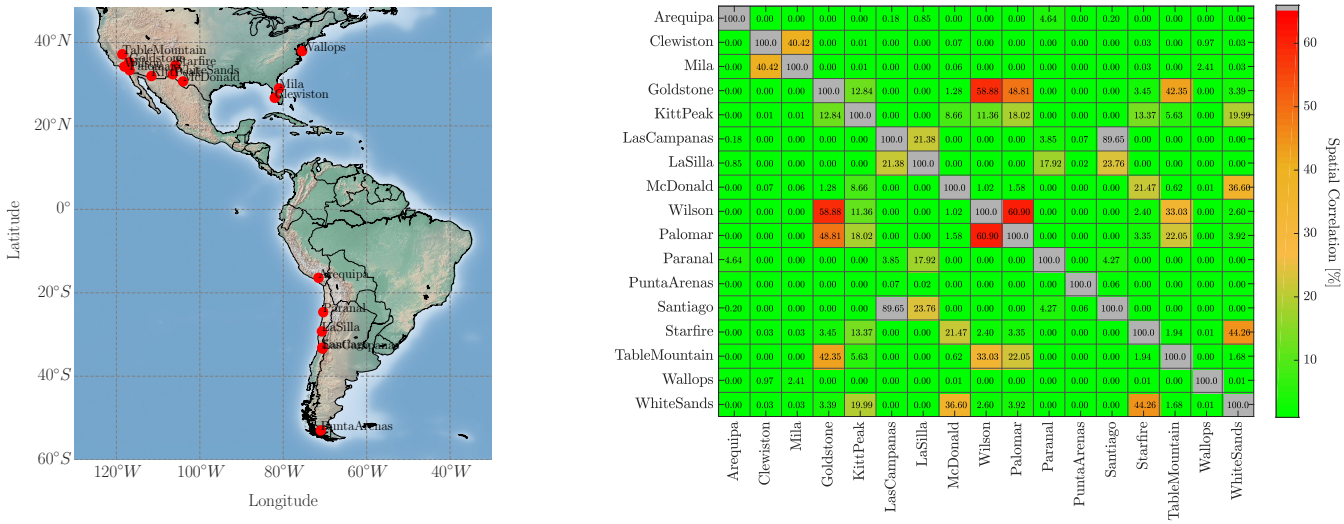

(a) **Candidate Ground Stations**

(b) **Spatial Correlation**

Figure 4: **Ground Segment for Geosynchronous Scenario**

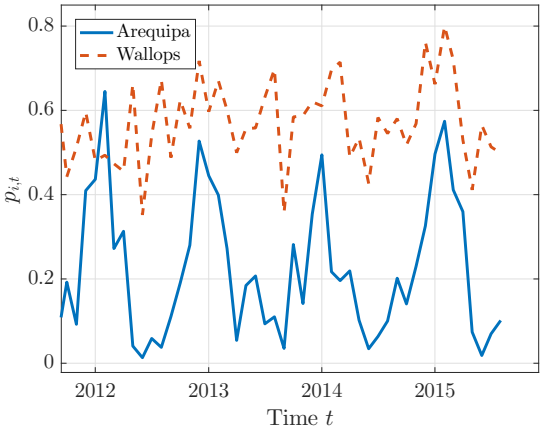

Figure 5: **Cloud Fraction Time Series**

ingly, we observe that the link-switched architecture has better performance than the multiplexed alternative regardless of the number of sites built. For instance, a network of 4-6 ground stations has almost perfect normalized throughput in the link-switched case, while the multiplexed case exhibits only 0.75 units of normalized throughput. Even more surprising is the fact that the performance of a multiplexed architecture decreases as more ground telescopes are included. In other words, as defined, a link-switched architecture is always better than a multiplexed system and spending more resources does not fix the problem.

To understand the rationale behind this finding, assume that a linked-switched system schedules a pass of T seconds at a rate of R_b bits per second. After t seconds, the link becomes clouded and is handed over to a second ground telescope that is cloud-free. Thanks to the assumption that this hand-off is error-free and instantaneous, the system has transmitted data continuously and the effect of clouds has been imperceptible, i.e. the total data volume transmitted is $R_b \cdot T$. Consider now the exact same scenario with two ground stations and a multiplexed optical payload. Until t seconds, the amount of data downlinked is exactly the same, although have of it goes to station 1 and the other half to station 2. After t, station 1 receives no data, but station 2 continues to receive information at a rate of $R_b/2$ bits per second. Consequently, the total data volume returned in the multiplexed case is $R_b \cdot t + \frac{R_b}{2}(T-t)$, a value strictly lower than $R_b \cdot T$ for $t < T$.

On the other hand, Figure 6b plots the multiplexing efficiency for the optimal multiplexed architectures. Observe that it decreases from 1 when there is only one ground telescope to approximately 60% when more than 15 sites are built. Three noteworthy remarks are possible:

- η is strictly decreasing with N. This is expected since more multiplexed downlinks result in less data rate per link and therefore less data returned when one of them fails. In other words, since there is no dynamic allocation of data onto active links, when a large set of them fail, less total throughput is being delivered to the ground. This is not the case in the link-switched architecture where the hand-off mechanism ensures that the high rate beam is always pointed to a non-clouded station.
- η can be used to quantify the data rate increase per link required in a link-switched architecture that has to provide a total capacity C to N ground stations simultaneously using a multiplexed system. In other words, the link data rate should be $R_b = \frac{C}{N \cdot \eta}$ to satisfy the capacity requirement on expectation and, at the same time, avoid the need for complex link switching mechanisms.
- η can be used to set the required performance for the link-switching mechanism. In other words, if a total capacity of C bits per second is required and N ground stations are available, then the link-switching protocol can only disrupt the downlink for up to $\eta \cdot C$ bits per second on expectation. Otherwise the capacity requirements will not be met.

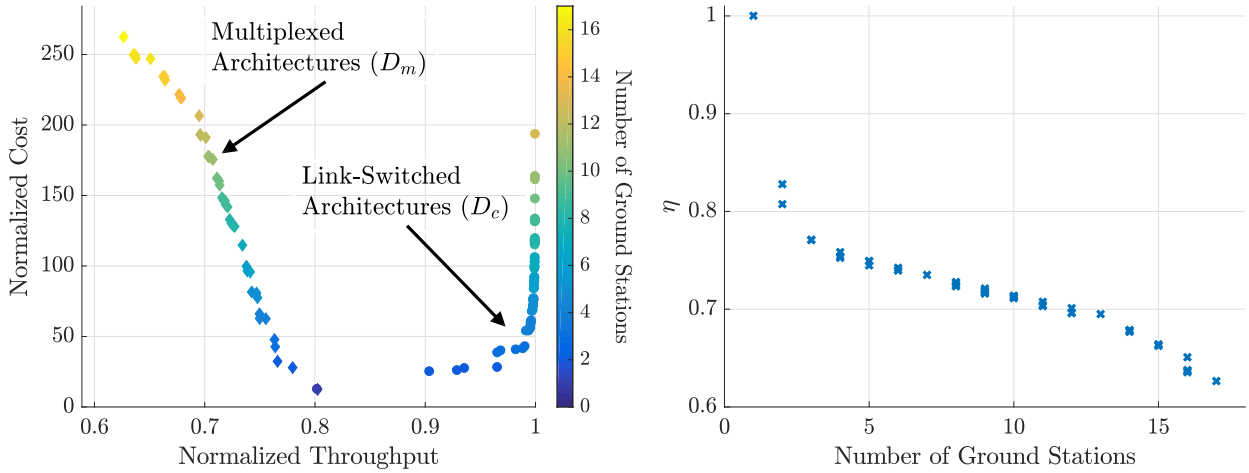

(a) **Link-Switched vs. Multiplexed Tradespace**

(b) **Multiplexing Efficiency**

Figure 6: **Ground Segment for Geosynchronous Scenario**

5. Low Earth Orbit Satellite Scenario

Scenario Description

In this scenario we evaluate the performance of link-switched and multiplexed network architecture when supporting a Low Earth orbit (LEO) spacecraft. Since high data volume satellites that image the Earth are typically flown in sun-synchronous orbits, we select the orbital parameters of the well-known Terra spacecraft [19] and compute its line of sight visibility periods with the set of ground stations from Figure 8a that lay in the West Coast and central part of the USA. Results are reported in Figure 7 during a week of the spacecraft's operations. We note that contact opportunities between network and spacecraft happen approximately twice per day assuming a minimum elevation angle of 10 deg.

Since LEO spacecraft fly at significantly lower altitudes than geosynchronous satellites, the set of ground stations that are in visibility with the spacecraft at any point in time is significantly reduced (both in number of telescopes and distance between them). Consequently, the average spatial correlation of telescopes supporting LEO spacecraft is significantly higher. This can be observed in the correlation matrix from Figure 8b where no ground station is perfectly uncorrelated with any other site. Furthermore, we can utilize Fuch's [4] definition of average network correlation

$$\bar{\lambda}_n = \frac{1}{\binom{N}{2}} \sum_{i=1}^{N-1} \sum_{j=i+1}^{N} \lambda_{i,j} \tag{17}$$

and average ground station correlation to quantify differences in spatial correlation between the GEO and LEO scenarios:

$$\bar{\lambda}_n = \frac{1}{N-1} \sum_{j=1, j\neq i}^{N} \lambda_{i,j}. \tag{18}$$

Table 1 reports the obtained results. Observe that the average correlation for all ground stations is higher in the LEO case as compared to the GEO case. Similarly, observe that the network average correlation in the LEO case is as high 46%, while it is only 18% in the GEO case.

Table 1: **Network and Ground Station Average Correlation**

Name	Scenario	
	LEO	GEO
Network	45.91%	17.62%
Arequipa	-	0.37%
Clewiston	-	2.60%
Florida Ground Station	-	2.68%
Goldstone	24.43%	10.69%
Kitt Peak	12.84%	5.62%
Las Campanas	-	7.20%
La Silla	-	4.00%
McDonald Observatory	10.18%	4.46%
Mount Wilson	24.31%	10.64%
Palomar	22.66%	9.91%
Paranal Chile	-	1.92%
Punta Arenas	-	0.01%
Santiago Satellite	-	7.37%
Starfire Optical	12.89%	5.64%
Table Mountain	15.33%	6.70%
Wallops Flight Facility	-	0.21%
White Sands	16.06%	7.03%

Finally, in order to evaluate the performance of a multiplexed architecture and compare it against a traditional link-switched system for a LEO scenario, we proceed analogously to Section 4. Using the same binary vector of 0/1s, we create a network by selecting a set of ground stations from the 8 available sites. Then, we estimate ONA_t and $\bar{X}_t$ using the cloud fraction data set and the lyapunov CLT and correlated MCS methods, as well as Equations 7 and 9.

Link-Switched vs. Multiplexed Architecture

Figure 9 presents the results of the LEO scenario in the normalized throughput-cost space. To facilitate comparison

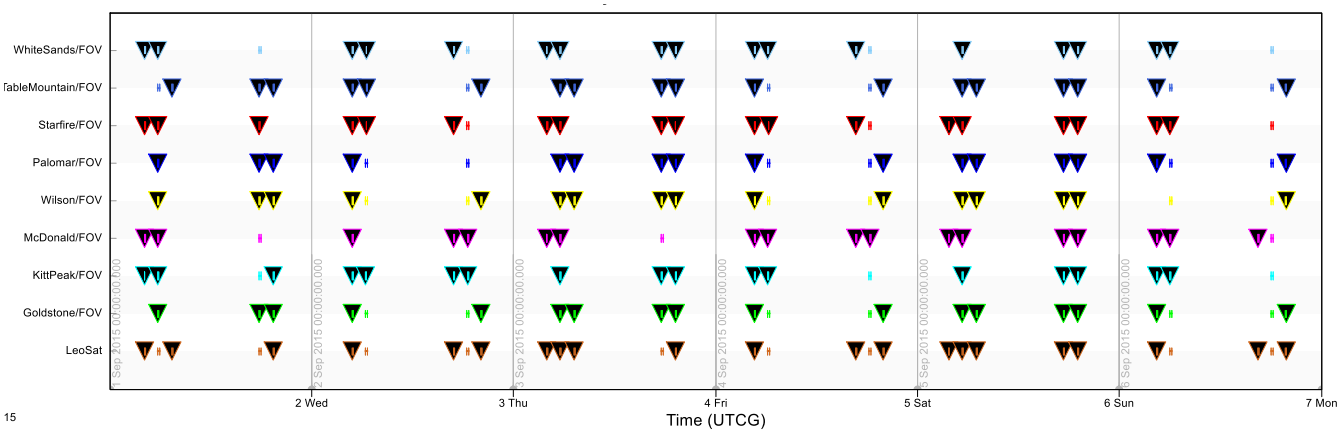

Figure 7: **Contact Opportunities between LEO Spacecraft and Ground Network**

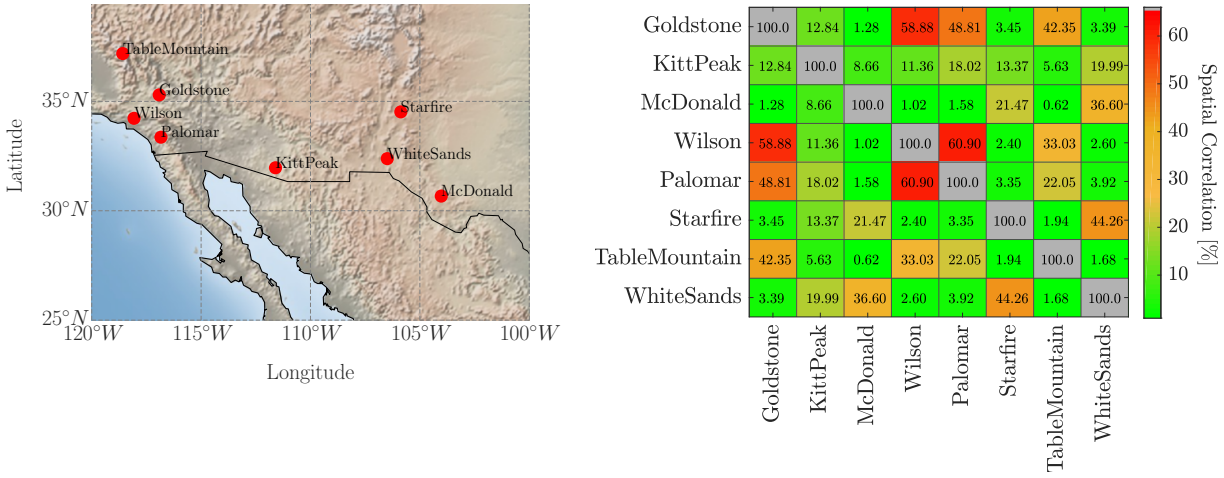

(a) **Candidate Ground Stations**

(b) **Spatial Correlation**

Figure 8: **Ground Segment for LEO Scenario**

between both scenarios, four plots are provided: The link-switched and multiplexed Pareto-optimal systems in the LEO case, and the same plots for the GEO case. It is important to mention that the comparison herein presented assumes that the GEO and LEO satellites are operated using the same communication profile: One contact per month, of arbitrary duration and data rate. It could be argued that the GEO satellite would, in fact, be communicating with the ground system continuously since it is always within line-of-sight from the ground stations. While this argument is true, it would also result in a linear increase of the returned data volume, and therefore would be irrelevant for comparison across scenarios.

The blue dots and diamonds from Figure 9a present the Pareto-optimal architectures for the ground segment of the LEO scenario when assuming a link-switched and multiplexed system respectively. To assess the effect of spatial correlation in the system performance, we first center our attention towards the difference between orange and blue dots. Observe that regardless of the system architecture, the geosynchronous scenario always results in larger normalized throughput. This is primarily due to the deleterious effect of ground site correlation for geographically close sites. In that sense, an average increase in ground site correlation of 30% approximately, results in a performance degradation of 0.01-0.03 units of normalized throughput or, equivalently, a reduction in data volume of 1 to 3%.

On the other hand, Figure 9b plots the multiplexing efficiency for the both the LEO and GEO scenarios. Observe that, in this case, there is not a significant difference between them, with efficiencies of 70% to 80% being typical if less than 8 sites are considered. This indicates that, to first order approximation, selection of a link-switched vs. multiplexed architecture can be performed independently from the site selection process.

6. Conclusions

Summary

In this paper we characterized and studied the trade-off between performance and cost for networks of telescopes that support both LEO and GEO spacecraft. Two main space-to-ground optical technologies have been considered: A link-switched architecture in which the spacecraft has the ability to create one unique downlink towards a non-clouded telescope;

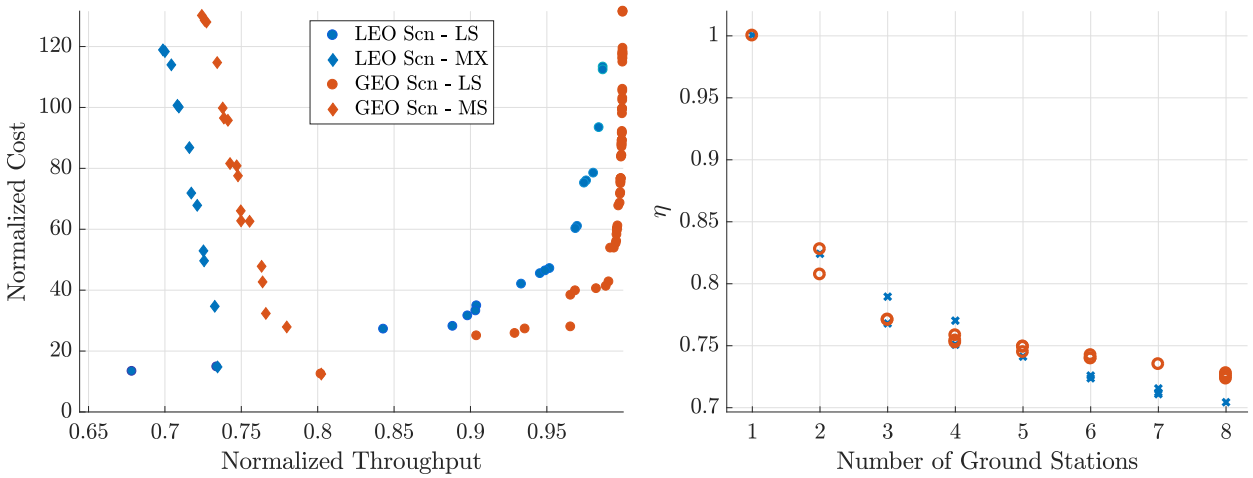

(a) **Link-Switched vs. Multiplexed Tradespace**

(b) **Multiplexing Efficiency**

Figure 9: **Ground Segment for Geosynchronous Scenario**

and a multiplexed system in which N downlinks at lower data rate are established simultaneously through a multiple access optical payload.

Three main research goals were addressed by this paper: First, we derived mathematical expressions for the expected data volume per pass as a function of the architecture (number of ground sites, linked-switched vs. multiplexed) and cloud statistics. Second, we quantified the difference in performance and cost when supporting a GEO and LEO satellite due to cloud correlation. Third, we assessed the efficiency of a multiplexed architecture with respect to a traditional link-switched system.

Results indicate that cloud-correlation between geographically close sites can reduce the expected capacity of a space-to-ground optical system by as much as 3%. This must be particularly considered for systems that are designed to service LEO satellites with limited field-of-view. On the other hand, we have demonstrated that multiplexed architectures that do not require complex link-switching mechanisms result in performance loss of 60% to 80% depending on how many downlinks and ground stations are available simultaneously. This performance loss is primarily attributable to the lack of a dynamic control mechanism that is able to predict cloud coverage and point the downlink towards a non-clouded ground station.

Future work

Multiple areas of future work are possible. On the one hand, the proposed data volume characterization is restricted to the first moment, i.e. the expectation. Quantifying higher moments or characteristic values such as the 95% confidence interval should also be considered, as they provides valuable information towards ensuring that the network is able to meet its customer requirements a high percentage of time. On the other hand, better characterization of the differences between a single and multiple access optical space terminals would also be beneficial. For instance, in this paper we have assume that the mass and cost of these two technologies is approximately the same. If that is not the case, then these differences should be taken into account when quantifying the performance-cost tradespace. Finally, network reliability against optical hardware failures should also be incorporated in the analysis. Indeed, a multiplexed system with large number of ground stations degrades gracefully if part of the space-to-ground links malfunction, while a link-switched architecture does not necessarily exhibit this property.

APPENDIX

Table 2 summarizes the location and normalized life cycle cost for the different ground stations considered in the two case studies of this paper. The provided values assume that a ground station has a construction cost of $1, a recurring cost of $0.40, and a life time of 30 years. Recurring costs escalate at a rate of 2% annually and are discounted at a 1% rate.

REFERENCES

[1] D. M. Boroson, J. J. Scozzafava, D. V. Murphy, B. S. Robinson, and M. Lincoln, "The lunar laser communications demonstration (llcd)," in *Space Mission Challenges for Information Technology, 2009. SMC-IT 2009. Third IEEE International Conference on*. IEEE, 2009, pp. 23–28.

[2] R. Link, M. E. Craddock, and R. J. Alliss, "Mitigating the impact of clouds on optical communications," in *2005 IEEE Aerospace Conference*. IEEE, 2005, pp. 1258–1265.

[3] G. S. Wojcik, H. L. Szymczak, R. J. Alliss, R. P. Link, M. E. Craddock, and M. L. Mason, "Deep-space to ground laser communications in a cloudy world," in *Optics & Photonics 2005*. International Society for Optics and Photonics, 2005, pp. 589 203–589 203.

[4] C. Fuchs and F. Moll, "Ground station network optimization for space-to-ground optical communication links," *Journal of Optical Communications and Networking*, vol. 7, no. 12, pp. 1148–1159, 2015.

[5] S. Poulenard, B. Roy, M. Hanna, H. Lacoste, and A. Rissons, "Optical ground station network optimization and performances for high data rate geosatellite-to-

Table 2: **Normalized Life Cycle Cost for Geosynchronous and Low Earth orbit Scenario**

Name	Country	Latitude	Longitude	Altitude	Life Cycle Cost
Arequipa	Peru	-16.4	-71.5	2321	12.44
Clewiston	Florida, USA	26.7	-82.0	3	12.54
Florida Ground Station	USA	29.0	-81.0	0	12.77
Goldstone	California, USA	35.3	-116.9	987	19.91
Kitt Peak	Arizona, USA	32.0	-111.6	1991	14.79
Las Campanas	Chile	-33.4	-70.6	688	15.48
La Silla	Chile	-29.3	-70.7	2332	15.48
McDonald Observatory	Texas, USA	30.7	-104.0	2001	13.31
Mount Wilson	California, USA	34.2	-118.1	1728	18.97
Palomar	California, USA	33.4	-116.8	1780	18.22
Paranal Chile	Chile	-24.6	-70.4	2065	15.48
Punta Arenas	Chile	-53.0	-71.0	88	15.48
Santiago Satellite Station	Chile	-33.1	-70.7	698	15.48
Starfire Optical Range	New Mexico, USA	34.5	-105.9	1950	13.86
Table Mountain	California, USA	37.2	-118.6	2719	18.22
Wallops Flight Facility	Virginia, USA	37.9	-75.5	11	15.11
White Sands	New Mexico, USA	32.4	-106.5	1313	14.94

ground telemetry," in *Proc. of 6th ESA Int. Workshop on Tracking, Telemetry and Command Systems for Space Applications*, 2013.

[6] N. Kura, M. Toyoshima, and Y. Takayama, "Estimation of accessible probability in a low earth orbit satellite to ground laser communications," *Radioengineering*, 2010.

[7] I. O. A. Group, "Optical link study group final report," Tech. Rep., 2012.

[8] O. Shibata, K. Inagaki, Y. Karasawa, and Y. Mizuguchi, "Spatial optical beam-forming network for receiving-mode multibeam array antenna-proposal and experiment," *IEEE Transactions on Microwave Theory and Techniques*, vol. 50, no. 5, pp. 1425–1430, 2002.

[9] N. Perlot and J. Perdigues-Armengol, "Model-oriented availability analysis of optical geo-ground links," in *SPIE LASE*. International Society for Optics and Photonics, 2012, pp. 82 460P–82 460P.

[10] M. S. Net, I. del Portillo, E. Crawley, and B. Cameron, "Approximation methods for estimating the availability of optical ground networks," *Journal of Optical Communications and Networking*, vol. 8, no. 10, pp. 800–812, 2016.

[11] M. Sanchez, I. del Portillo, B. G. Cameron, and E. F. Crawley, "Architecting space communication networks under mission demand uncertainty," in *2015 IEEE Aerospace Conference*. Big Sky, Montana: Institute of Electrical and Electronics Engineers, March 7-14 2015.

[12] S. Spangelo and J. Cutler, "Analytical modeling framework and applications for space communication networks," *Journal of Aerospace Information Systems*, vol. 10, no. 10, pp. 452–466, 2013.

[13] E. P. S. Office. Nasa earth observations - cloud fraction. [Online]. Available: http://neo.sci.gsfc.nasa.gov

[14] P. Garcia, A. Benarroch, and J. M. Riera, "Spatial distribution of cloud cover," *International Journal of Satellite Communications and Networking*, vol. 26, no. 2, pp. 141–155, 2008.

[15] U. F. Criteria, "Dod facilities pricing guide," Department of Defense, Tech. Rep., March 2015.

[16] O. L. S. Group, "Optical link study group final report," Interagency Operations Advisory Group, Tech. Rep., June 2012.

[17] I. del Portillo, M. Sanchez, B. G. Cameron, and E. F. Crawley, "Architecting the ground segment of an optical space communication network," in *2016 IEEE Aerospace Conference*, 2016.

[18] W. Tai, N. Wright, M. Prior, and K. Bhasin, "Nasa integrated space communications network," in *Proceedings of Space Ops 2010 Conference, AIAA*, 2012.

[19] A. Ignatov, I. Laszlo, E. Harrod, K. Kidwell, and G. Goodrum, "Equator crossing times for noaa, ers and eos sun-synchronous satellites," *International Journal of Remote Sensing*, vol. 25, no. 23, pp. 5255–5266, 2004.

BIOGRAPHY

Marc Sanchez Net *is currently a fourth year Ph.D. candidate in the department of Aeronautics and Astronautics at MIT. His research focuses on architecting space communication networks to support future space exploration activities. He has interned twice at NASAs Jet Propulsion Laboratory in the Communication Architecture and Research Section. He received his M.S. in aeronautics and astronautics in 2014 from MIT, and also holds degrees in both telecommunications engineering and industrial engineering from Universitat Politecnica de Catalunya, Barcelona.*

Iñigo del Portillo *is a graduate student in the department of Aeronautics and Astronautics at MIT. His research interests include optical communications for space-based networks and small satellites communications. Iñigo received his degrees in Industrial Engineering, Electronics Engineering and Telecommunications Engineering in 2014 from Universitat Politecnica de Catalunya, Barcelona.*

Dr. Bruce Cameron *is a Lecturer in Engineering Systems at MIT and a consultant on platform strategies. At MIT, Dr. Cameron ran the MIT Commonality study, a 16 firm investigation of platforming returns. Dr. Cameron's current clients include Fortune 500 firms in high tech, aerospace, transportation, and consumer goods. Prior to MIT, Bruce worked as an engagement manager at a management consultancy and as a system engineer at MDA Space Systems, and has built hardware currently in orbit. Dr. Cameron received his undergraduate degree from the University of Toronto, and graduate degrees from MIT.*

Dr. Edward F. Crawley *received an Sc.D. in Aerospace Structures from MIT in 1981. His early research interests centered on structural dynamics, aeroelasticity, and the development of actively controlled and intelligent structures. Recently, Dr. Crawleys research has focused on the domain of the architecture and design of complex systems. From 1996 to 2003 he served as the Department Head of Aeronautics and Astronautics at MIT, leading the strategic realignment of the department. Dr. Crawley is a Fellow of the AIAA and the Royal Aeronautical Society (UK), and is a member of three national academies of engineering. He is the author of numerous journal publications in the AIAA Journal, the ASME Journal, the Journal of Composite Materials, and Acta Astronautica. He received the NASA Public Service Medal. Recently, Prof Crawley was one of the ten members of the presidential committee led by Norman Augustine to study the future of human spaceflight in the US.*